3D patterning/manipulating microparticles and yeast cells using ZnO/Si thin film surface acoustic waves

Xiang Tao,[a,b] Tan Dai Nguyen,[c] Hao Jin,[*,a] Ran Tao,[b] Jingting Luo,[d] Xin Yang,[e] Hamdi Torun,[b] Jian Zhou,[f] Shuyi Huang,[a] Lin Shi,[a] Des Gibson,[g] Michael Cooke,[h] Hejun Du,[c] Shurong Dong,[a] Jikui Luo,[a] YongQing Fu [b]

[a] *College of Information Science and Electronic Engineering, Zhejiang University, Hangzhou 310027, China*
[b] *Faculty of Engineering and Environment, Northumbria University, Newcastle upon Tyne, NE1 8ST, UK*
[c] *School of Mechanical and Aerospace Engineering, Nanyang Technological University, 639798, Singapore*
[d] *College of Physics and Energy, Shenzhen Key Laboratory of Sensor Technology, Shenzhen University, 518060, People's Republic of China*
[e] *Department of Electrical and Electronic Engineering, School of Engineering, Cardiff University, UK CF24 3AA*
[f] *College of Mechanical and Vehicle Engineering, Hunan University, Changsha 410082, P. R. China*
[g] *Institute of Thin Films, Sensors & Imaging, University of the West of Scotland, Scottish Universities Physics Alliance, Paisley PA1 2BE, UK*
[h] *Department of Engineering, Durham University, South Road, Durham, DH1 3LE, UK*

Keywords: Acoustofluidic, ZnO, 3D manipulation, Yeast cell, Lab on a chip

Abstract

Manipulating biological cells or microparticles in three dimensions (3D) is invaluable for many biomedical applications, and recently effective and rapid manipulations of microparticles in 2D and 3D within microchannels or chambers using surface acoustic waves (SAWs) with bulk piezoelectric materials have been reported. However, these are generally expensive, or brittle and cannot be easily integrated into a single lab-on-chip. In this paper, we realized microparticle/cell patterning and 3D manipulation of yeast cells inside a chamber with a height of 1 mm using thin film ZnO/Si SAW devices. Effects of SAW frequency, channel width and thickness on alignment of microparticles were firstly investigated, and positions of the microparticles in the direction of SAW propagation

* Corresponding author.
E-mail address: hjin@zju.edu.cn (Hao Jin)

can be controlled precisely by changing the phase angle of the acoustic waves from the ZnO/Si SAW device. A numerical model has been developed to investigate the SAW acoustic field and the resulted 3D motions of microparticles under the acoustic radiation forces within the microchamber. Finally, we realized and observed the 3D patterning of yeast cells within the microchannel. Our work shows a great potential for acoustofluidic, neural network research and biomedical applications using the ZnO/Si SAW devices.

1. Introduction

Surface acoustic wave (SAW) devices have recently been extensively investigated for microfluidic applications as they are capable of handling liquid in extremely low volume, manipulating and patterning micro-sized biological objects in liquid precisely and efficiently within microchannels or chambers [1–4]. The SAW devices are biocompatible, versatile, low-cost, simple in design, contactless, and the manipulation is non-invasive and efficient [1,2,5], making them an extremely attractive choice for manipulation of biological cells. Furthermore, SAW devices based on piezoelectric thin film materials such as ZnO [6] and AlN [7] could be seamlessly integrated into a single lab-on-chip (LOC) device at a low cost [8]. Numerous researchers have achieved effective and rapid manipulations of microparticles forming one dimensional (alignment) and two dimensional (matrix) patterns by using standing surface acoustic waves (SSAWs) [9,10]. For example, Shi *et al*. [11] achieved aligned microparticles in a microchannel positioned between two interdigitated transducers (IDTs) in which the SSAW was established. Microparticles in the SSAW were driven by a primary acoustic radiation force that is dependent on the microparticle size, density, and compressibility [12–14]. Ding *et al*. [16] utilized a SSAW-based tunable device to precisely sort single cells in a flow stream into as many as five separate outlet channels by manipulating phases of SSAW. Recently there are extensive work in this field to realize the precise manipulations of microparticles and cells in the microchannels [4,5,9,17–19].

Although the main focus in the literature is on the 2D manipulation of microparticles in the horizontal plane within the channel, initial work to manipulate the microparticles in three dimensions (3D) have been achieved [2]. Shi *et al*. [20] proved that SSAW could be effectively applied to achieve 3D manipulation; however the acoustic radiation force acting in the vertical

direction (z direction) is weaker than that acting in the device plane, and the manipulation of microparticles was demonstrated at a vertical range of only 100 μm. Whereas recently we have successfully demonstrated the manipulation in 3D in a vertical range of ~1 mm in the microchamber using the SSAW [1].

Currently the substrates of the SAW devices used in the particle/cell manipulations are mostly bulk piezoelectric materials such as $LiNbO_3$. Bulk piezoelectric materials usually have good piezoelectric coefficient and electromechanical coupling coefficients that results in high energy transduction efficiency [21]. However, they are generally expensive, brittle and cannot be easily integrated with electronics for control and signal processing [22]. It is therefore desirable to have thin film piezoelectric materials such as ZnO and AlN[23] to develop SAW devices for future acoustofluidic and LOC applications [22], and they are capable of integrating multiple functions onto different substrates such as silicon (Si), glass, metal, or polymer [24,25]. As an emerging application, it is highly desired to explore the 3D patterning and manipulation of microparticles/cells using the thin film SAW devices.

This paper will demonstrate patterning and manipulating of polystyrene microspheres and yeast cells inside a 1mm height chamber using ZnO/Si SAW device. The work has shown the potential of using ZnO/Si SAW device as a novel tool in biomedicine, tissue engineering, neuron network and regenerative medicine. In addition, we investigated the effects of SSAW frequency, channel width and thickness on patterning microparticles. We have also achieved precise position control of the microparticles along the SSAW propagation by changing the phase angles of the SAW. Moreover, we used a numerical model to investigate the SAW acoustic field and the microparticle trajectories inside the PDMS chamber.

2. Material and Methods

Fig. 1(a) shows the schematic of the experimental apparatus for observing 3D lines of yeast cell microparticles, and Fig. 1(b) shows the top view of ZnO/Si SAW device bonded with the micro-chamber used in our study. A ZnO film of ~5.5 μm thick was deposited onto a silicon (100) substrate using standard DC magnetron sputtering (Nordico Sputter System). The IDTs were also patterned by the same technique by sputtering 150 nm aluminum and using a lift-off process. Three ZnO/Si SAW devices with the wavelengths of 100, 200 and 400 μm were manufactured and investigated.

The Rayleigh mode of the SAW devices were characterized using a network analyzer (HP8752A), with the reflection spectra shown in Fig. S1 in the supplementary material. The resonant frequencies of these three devices are 42.2, 24.0 and 12.2 MHz respectively. PDMS channels (Sylgard 184 Silicone Elastomer; Dow Corning, USA) of different widths and thicknesses were fabricated for bonding to the ZnO/Si SAW devices for testing. A cuboid PDMS chamber (1.5 mm (L) ×1.5 mm (W) ×1.0 mm (H)) was also prepared to investigate the 3D manipulation of microparticles and yeast cells. Three different sized polystyrene microspheres with diameters of 0.5 μm, 6 μm and 10 μm (Sigma Aldrich Ltd) and yeast cells (Bake King Instant Yeast) with an average diameter of ~4 μm were used for the experiment. A syringe pump (LSP02-1B dual-channel syringe pump; LongerPump, China) was used for injecting liquid samples to the device. For the 3D yeast cell manipulation, we connected a charge-coupled device (CCD) camera (Andor iXonEMt; Oxford Instruments, UK) to a microscope (Eclipse Ti-U inverted microscope; Nikon, Japan) to observe the microparticle trajectories. In order to record the vertical microparticle motions, we used a right-angle prism (N-BK7 right-angle prism; length of 1mm, Edmund Optics, USA) to reflect the light from the side of the microchannel to the microscope (Fig. 1(a)).

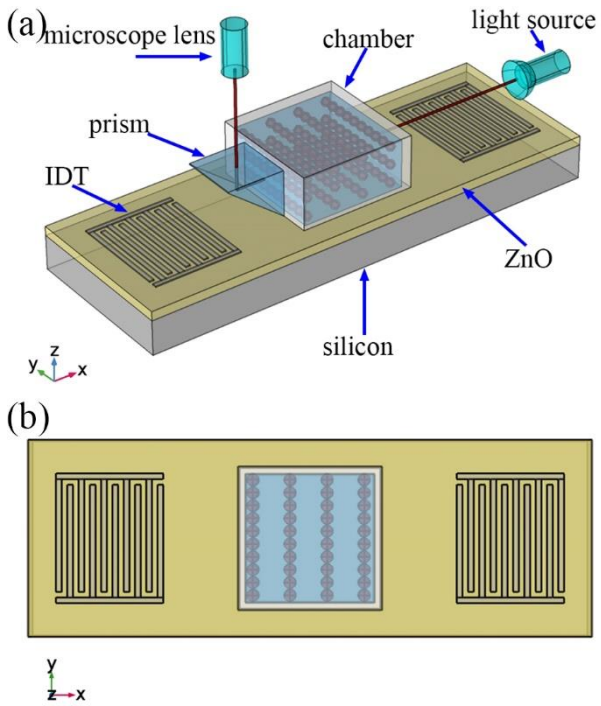

Fig. 1 (a) A schematic of the experimental setup for observing 3D lines of yeast cells from the side using the prism, (b) the top view of the experimental setup.

3. Results and discussions

3.1. Factors influencing microparticle manipulation in both 2D and 3D

3.1.1. SAW frequency

The width and the thickness of the PDMS microchannel used for exploring the frequency effect were 1,000 μm and 280 μm, respectively, and the size of polystyrene microsphere was 6 μm. When the same radiofrequency (RF) signals were applied to the two IDTs, two travelling SAWs counter-propagate and interfere with each other, resulting in a one-dimensional SSAW field [26], in which a series of pressure nodes (PNs) and anti-nodes (ANs) are formed in the microchannel at the interval of half SAW wavelength. Microparticles expressing positive acoustic contract factors will be driven toward the nearest PNs [26–28].

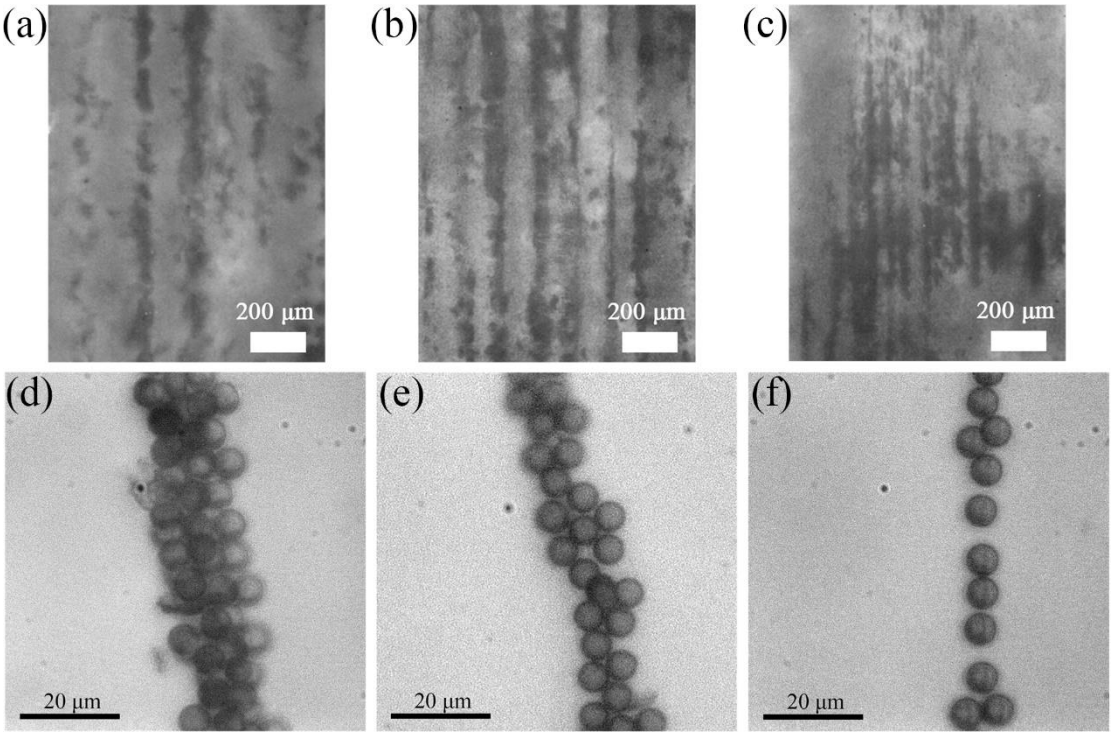

Fig. 2 The microparticles were aligned in the ZnO/Si SAW device working on the frequency of (a) 12.2 MHz, (b) 24.0 MHz, and (c) 42.2 MHz, the selected partially enlarged images of linear arrangements of microparticles under (d) 12.2 MHz, (e) 24 MHz, (f) 42.2 MHz respectively.

Figs. 2(a)-2(c) show the microparticle alignment using three frequencies of 12.2 MHz, 24.0 MHz and 42.2 MHz, respectively. Once the RF signal was applied to the IDTs, the microparticles were actuated by the SSAWs and aligned precisely in the channel. The corresponding wavelengths were 400 μm, 200 μm, and 100 μm, which agree with distances of adjacent microparticle traces of

$\lambda_{SAW}/2$, where λ_{SAW} is the wavelength of the SAW device. Figs. 2(d)-(f) shows the selected examples of partially enlarged images for the aligned microparticles actuated under the three frequencies. In many cases, the width of the microparticle trace was found to decrease with the increase of the frequency, and the widths of the traces in Fig 2 are about 17.7±2 μm, 12.1±1.8 μm, 6.0±1.2 μm, respectively.

When the SAW is established in the fluid medium, the microparticle suspension experiences primary acoustic radiation forces that drive the microparticles toward either PNs or ANs. Microparticles will also experience a viscous force when they move. The primary acoustic radiation force (which is a function of the microparticles properties) and the viscous force can be described as [15,29]:

$$F_a = -\left(\frac{\pi p_0^2 V_p \beta_l}{2\lambda}\right)\phi(\beta,\rho)\sin(2kx) \tag{1}$$

$$\phi = \frac{5\rho_p - 2\rho_l}{2\rho_p + \rho_l} - \frac{\beta_p}{\beta_l} \tag{2}$$

$$p_0 = \sqrt{\alpha \frac{p_{in}\rho_s c_s}{A_w}} \tag{3}$$

$$F_v = -6\pi\eta r v \tag{4}$$

where F_a corresponds to the acoustic radiation force, p_0 is the acoustic pressure, V_p the microparticle volume, λ the wavelength, k the wave number, x distance of the microparticle from the PN, ρ_l the density of medium, ρ_p the density of microparticles, β_l the compressibility of medium, β_p the compressibility of microparticles, F_v the viscous force, η the medium viscosity, r microparticle radius, and v the relative velocity, respectively. The acoustic pressure is given by Eq. 3, where α is the power conversion factor, p_{in} the input power, ρ_s the density of ZnO/Si substrate, c_s the phase velocity of SAW in ZnO/Si substrate and A_w the working area (IDT length multiplied by the distance between two IDT), respectively. All the microparticles are of the same density, compressibility and size. From Eq. 1, it is clear that higher frequency or smaller wavelength of the SAW device will lead to a larger acoustic radiation force

F_a. Meanwhile, smaller wavelength will also lead to a smaller pressure node region, which could capture fewer microparticles. This was demonstrated by Figs. 2(d)-2(f), where the microparticles are more concentrated to align at a higher SAW frequency.

3.1.2. Channel width and thickness

In order to investigate the effects of channel width on patterning microparticles, three channels of different widths (300 μm, 500 μm, and 1,000 μm) were chosen, while the thickness of the channel walls was fixed at 280 μm.

To study the wall thickness effect, the ZnO/Si SAW device with 12.2 MHz frequency was used. Three channels with different wall thicknesses were used, and they were: 280 μm, 430 μm and 610 μm in the thickness, respectively. The width of all three channels was fixed at 1,000 μm. The size of polystyrene microspheres in these experiments was about 6 μm.

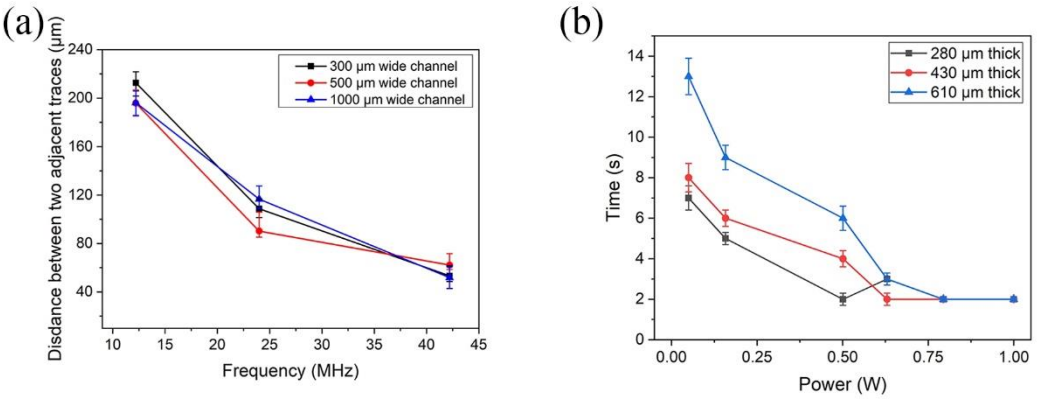

Fig. 3 (a) Distance (μm) between the adjacent lines when using the 300 μm, 500 μm, 1,000 μm channel widths with 12.2 MHz, 24.0 MHz and 42.2 MHz devices respectively, (b) the arrangement time required for channels with three wall thicknesses under different powers.

It can be seen from Fig. 3(a), when the frequency is increased, there is a decrease of the distance between the adjacent microsphere lines. The wavelength of 12.2, 24.0 and 42.2 MHz devices are 400 μm, 200 μm, and 100 μm, respectively, which are corresponding to the distance ($\lambda_{SAW}/2$) between adjacent traces. Influence of frequency could be exploited to adjust the distance of cells for cell analysis (e.g., cell-cell interaction) or the density of the pattern for bioengineering of tissue [30]. The experimental results agree with the theoretical prediction. Obviously, the width of the channel does not have much effect on the distance between two adjacent lines within the error range.

Fig. 3(b) shows the time required for microparticles to form aggregation under different input

powers. In general, thicker channel walls take the longer time for the microparticles to align because the PDMS material absorbs more acoustic energy when it is thicker. However, when the power is higher than 0.75 W, the time for alignment of the three channels is similar. This is because the PDMS attenuation becomes negligible when high acoustic power is applied.

3.1.3. Phase angle effect of the SAW

In all following experiments, we used the SAW device with a microchannel which was 280 µm thick and 1,000 µm wide. When microparticles in the channel are exposed to a SSAW field, the primary acoustic radiation force would drive and trap them to the nearest PN [2]. Once the microparticles are trapped on the PNs, they can be moved by changing the frequency or the phase angles of the applied RF signal [31–33]. We used 42.2 MHz SAW device to trap 6 µm and 10 µm microparticles on the PNs, by changing the phase of the RF signal supplying to one of the IDTs, the microparticles were shifted around the PN.

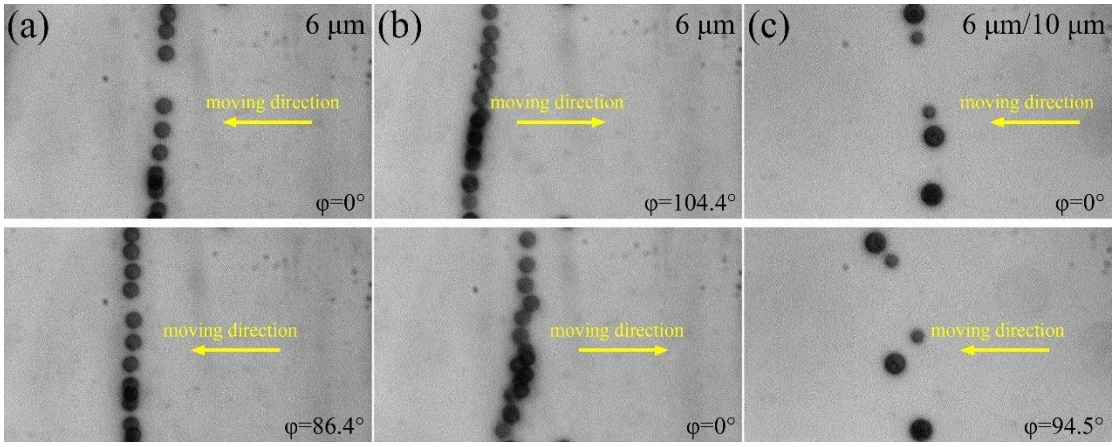

Fig. 4 Microparticle manipulation for two different sizes. (a) The manipulation of microparticle of size 6 µm by changing the phase angle from 0° to 86.4°. (b) The manipulation of microparticle of size 6 µm by changing the phase angle from 104.4° to 0°. (c) The manipulations of two microparticles of size 6 µm and 10 µm by changing the phase angle from 0° to 94.5°.

It can be seen from Fig. 4(a), the 6 µm microparticles are moved to the left side after changing the phase angle. Whereas Fig. 4(b) shows that 6 µm microparticles are moved to the right side. Finally, Fig. 4(c) show the movement of 6 µm and 10 µm microparticles moving to left side, and the displacements of 10 µm microparticles are much larger than the displacements of 6 µm

microparticles at a certain time (i.e., 10 μm microparticles move faster than 6 μm microparticles).

We define the right side as the positive direction of the displacement, and the theoretical relation between the displacement of microparticles manipulated and the phase-shift has been reported as following [3]:

$$\Delta x = -\frac{\lambda}{720^\circ}\Delta\varphi, \quad \Delta\varphi \in [-180^\circ, 180^\circ] \tag{5}$$

where Δx, λ and $\Delta\varphi$ correspond to the displacement of microparticle, wavelength and phase-shift, respectively. The experimental and calculated displacement of the 6 μm microparticles is shown in Fig. 5, which covers the phase shifting from -180° to 180°. The experimental displacement is changed almost linearly with the phase-shift, which is in a good agreement with the theoretical result. Obviously, the positions and trajectory of the microparticles in the direction of SAW propagation can be precisely controlled by adjusting the phase angle, which is invaluable in lab-on-a-chip systems.

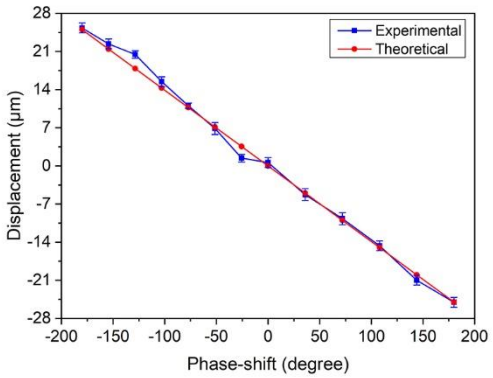

Fig. 5 The experimental and theoretical displacement of the 6 μm microparticles as a function of phase-shift.

3.1.4. Microparticle size effect

The size of microparticles has an influence on manipulation speed, which can be explained by Eq. 1 and Eq. 4. In these experiments, all microparticles were of the same density and compressibility, but with different sizes. As the acoustic force is proportional to the volume (r^3) of the microparticles, and the viscous force is proportional to the radius (r) of the microparticles, the larger the microparticle is, the higher the net force is, and faster the migration is [34]. When the microparticle maintains constant velocity in the SSAW field, the acoustic and viscous forces balance

each other [15,35]. Base on Eq. 1 and Eq. 4, we can get the velocity of microparticle.

$$v = -\left[p_0^2 V_p \beta_l / (12\lambda\eta r) \right] \phi(\beta, \rho) \sin(4\pi x / \lambda) \tag{6}$$

Rewriting $v = -dx/dt$ and separating variables:

$$\csc(4\pi x / \lambda)\, dx = \left[p_0^2 V_p \beta_l / (12\lambda\eta r) \right] \phi(\beta, \rho)\, dt \tag{7}$$

By integrating dx, we can get the relationship between displacement and time [15].

$$t = (3\lambda^2 \eta r) \ln\left(\tan(2\pi x / \lambda)\right) / \left[p_0^2 V_p \beta_l \pi \phi(\beta, \rho) \right], \qquad x \in (0, \lambda/4) \tag{8}$$

As shown in Fig. 6(a), the theoretical amplitude of the acoustic radiation force exerted on 6 μm microparticles is larger than that on 0.5 μm microparticles. Therefore, 6 μm microparticles move towards the pressure lines faster than 0.5 μm microparticles (Fig. 6(b) and (d)). We chose one 6 μm microparticle and one 0.5 μm microparticle as a reference, and their position coordinates at different times are shown in Fig. 6(b) and (d). We tracked the trajectories of the two microparticles by video for 0.25 s. The yellow arrow shows the microparticle moving direction. Obviously, from Fig. 6(b) to Fig. 6(d), the displacements of the 6 μm microparticle and the 0.5 μm microparticle are 33.8 μm, 9.0 μm, respectively. The displacements of microparticles of different sizes versus time are shown in Fig. 6(c), and the relative distance between two microparticles is ~26.2 μm in 0.25 s, which agrees well with the experimental result observed in Figs. 6(b) and 6(d). Therefore, the 6 μm microparticles move towards the pressure node much faster than smaller ones.

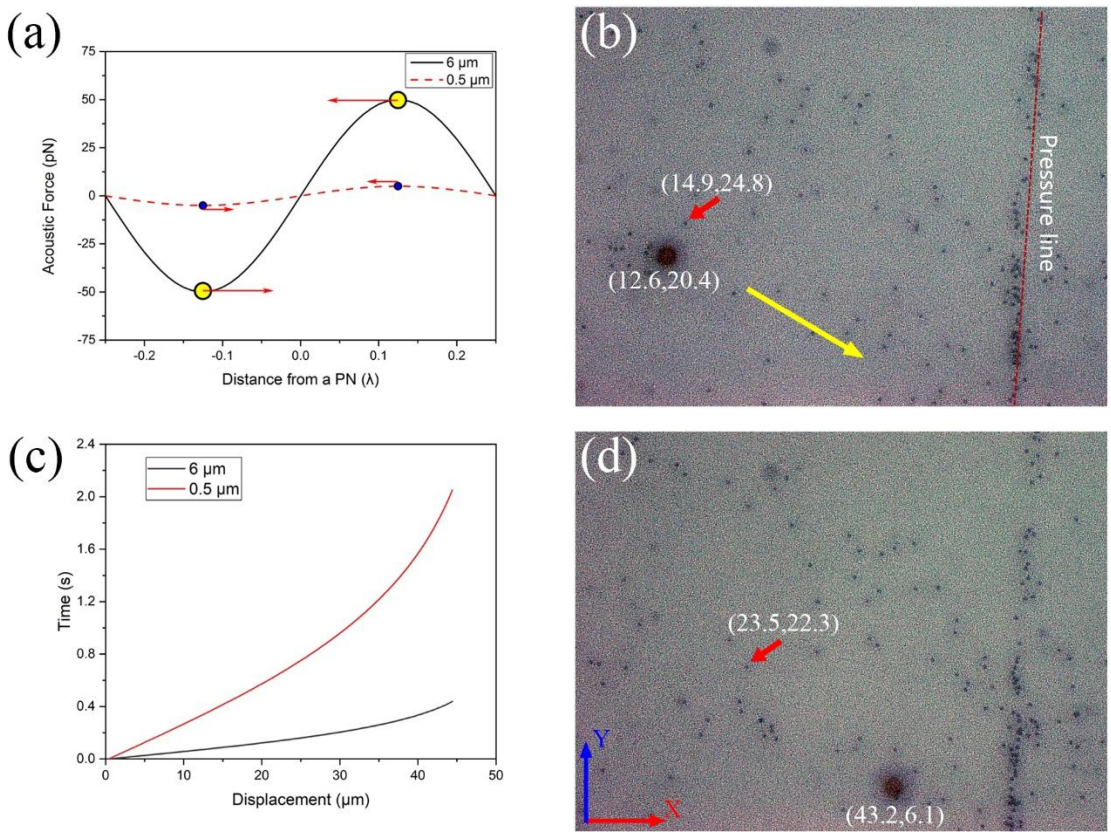

Fig. 6 (a) Primary acoustic force distribution along a SSAW wavelength. (b) and (d) Two different sizes of microparticles (6 μm and 0.5 μm) move to the acoustic pressure line for a certain period. (c) The displacements of microparticles of different sizes versus time.

3.2. 3D manipulation of yeast cells

Yeasts are eukaryotic, single-celled microorganisms classified as members of fungus types [36,37]. The useful physiological properties of yeast have led to their uses in the field of biotechnology [38,39]. Furthermore, yeasts include some of the most widely used model organisms for genetics and cell biology [40,41]. Manipulating and patterning large numbers of cells such as yeast in fluid in the chamber using the SSAW, has important biomedical applications in microarrays, tissue engineering and regenerative medicine [4,5,18].

3.2.1. 3D force analysis for a yeast cell

Any microparticle present in acoustofluidics will experience four forces as shown in Fig. 8(a); on the x-z plane, the buoyancy force (F_b) and gravitation force (F_G) are normally negligible. In the x direction, the two equal and opposite components of the radiation forces (F_{ax}) cancel each

other. In the z direction, there are three types of forces (i.e., the components of the radiation forces F_{ay}, upward F_B and downward F_G) [1]. The sum of the gravitational and buoyancy forces is a net downward force

$$F_G - F_B = Vg\left(\rho_y - \rho\right) \tag{9}$$

where V is the volume of the yeast cell microparticle, g is the gravitational acceleration, ρ_y is the density of the yeast cell microparticle and ρ is the density of water. The sum of the z component of the radiation forces is a net upward force, which is dependent strongly on the vertical position of the microparticles (i.e., the higher the position, the weaker the force) and input power (i.e., the higher the input power, the higher the force) [1]. When the net upward force is equal to the net downward force, 3D lines of microparticles can form and the height of the 3D patterns can be increased by increasing the input power.

3.2.2. COMSOL simulation

We used the finite-element method integrated in a commercial software package (COMSOL) Multiphysics (Version 5.3) to investigate the acoustic radiation force exerted on the microparticles in the chamber. Because the SSAW is uniform along the propagation direction of the channel, we simplified the chamber in the simulations to a 2D rectangular domain with dimensions of 1.5 mm (W) ×1.0 mm (H). The bottom edge of the model was given an actuation boundary condition to simulate the substrate vibrating with a frequency of 12.2 MHz, and the other edges were given the impedance boundary condition to simulate the PDMS walls. We also considered the effects of gravitation force and buoyancy force in the model, and the radius and density of yeast cell were set to 4 μm and 583.33 kg/m^3, respectively. We used a module called “Pressure Acoustic” to solve the acoustic pressure field and used another module called “Particle Tracing” to track the yeast cells. The simulation results are shown in Fig. 7.

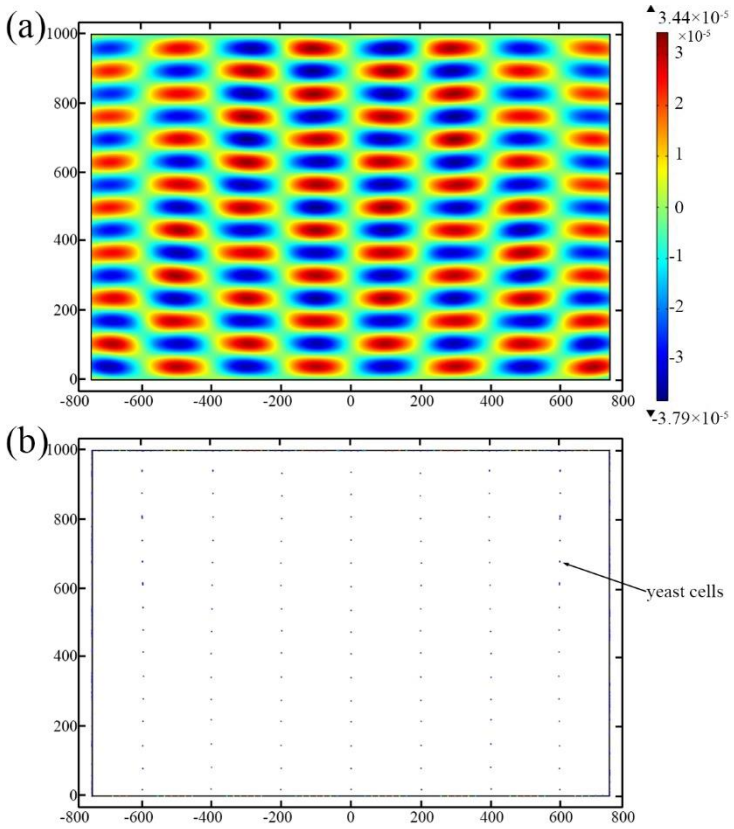

Fig. 7 (a) Acoustic pressure; colors show magnitude from -0.379 MPa (blue) to 0.344 MPa (red). (b) Numerical results for motion of yeast cells after 20 s.

As shown in Fig. 7(a), the acoustic pressure field is distributed periodically in both horizontal and vertical directions. The yeast cells would be driven to the area where the acoustic pressure is smallest (i.e., the green areas). Fig. 7(b) shows the final positions of yeast cells after applying power for 20 s. obviously, the yeast cells are distributed periodically in the chamber, with the distribution positions in a good agreement with the smallest acoustic pressure areas (Fig. 7(a)).

3.2.3. 3D line arrays

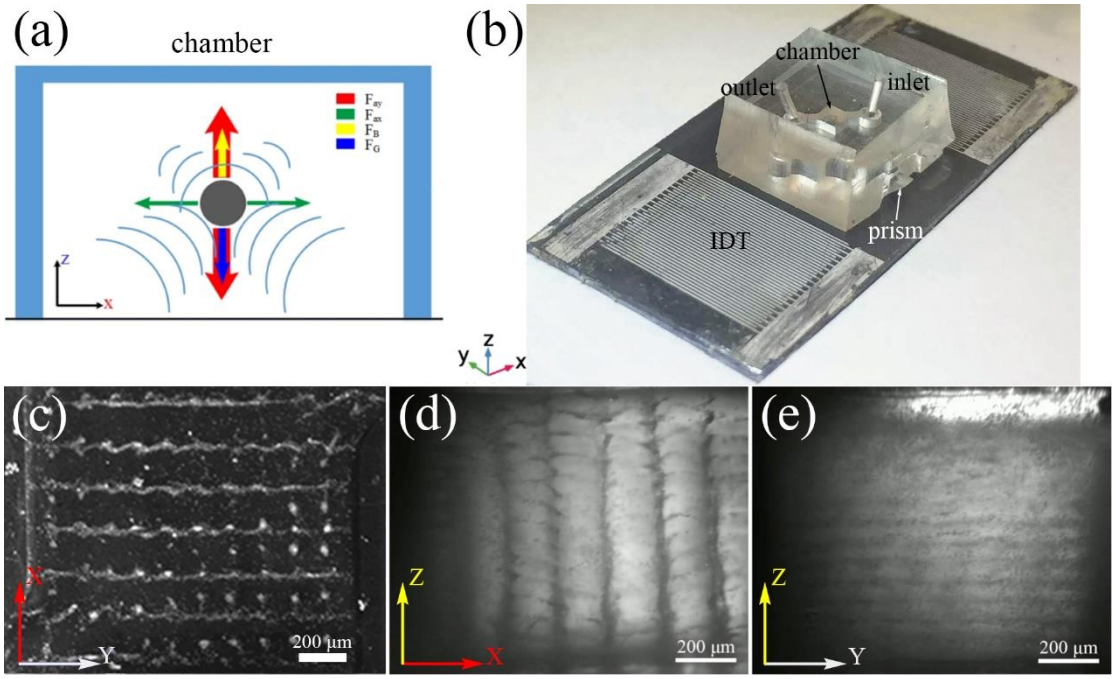

Fig. 8 (a) Force analysis for a yeast cells in the chamber. (b) Schematic of the experimental setup for observing 3D lines of yeast cells from the side using the prism. (c)–(e) Microscopy images of 3D lines of yeast cells after introducing an SSAW with an input power of 3500 mW viewed from z, y, and x directions, respectively.

Fig. 8(b) shows the experimental setup for observing 3D lines of yeast cells from the side using the prism. Figs. 8(c)–(e) show different views (along the z, y, and x directions, respectively) of the yeast cells in the chamber when yeast cells are patterned. The PDMS chamber is 1.5 mm (W) × 1.5 mm (L) × 1 mm (H). The wavelength and resonant frequency of the ZnO/Si SAW are 400 μm and 12.2 MHz, respectively. It can be seen from Fig. 8(c), the yeast cells are aggregated forming line pattern, and the distance between two adjacent lines is 200 μm, which is about half the wavelength of the device used. Approximately 7 lines are created over the chamber width. However, there are some dots between lines, caused by the chaining force between adjacent yeast cells. As shown in Fig. 8(d), the microparticles are also vertically aggregated forming separate lines at different height. Similarly, there are ~7 lines across the chamber length. There are wispy connections between the lines (Fig. 8(d)), which are the dots between line arrays as shown in Fig. 8(c). In the vertical direction, there are ~12 parallel lines of yeast cells with a distance of ~63 μm between two adjacent lines (Fig. 8(e)). The distance can be calculated approximately using $\lambda/2 = v/(2f)$, where λ is the

wavelength in the vertical direction, v is the speed of sound in water (~1502 m/s), and f is the operating frequency (12.2MHz). As the yeast cells have much large variation in the sizes, they are difficult to be aligned perfectly.

Due to the co-existence of the acoustic field and electric field in the chamber, yeast cells will experience two forces, the primary acoustic radiation force (F_a) generated by the SSAW and the chaining force by the AC electric field [42]. These cells will be polarized and interact with each other to form microparticles chain along the electric field lines (the x direction in Fig. 8(c)). The chaining force between adjacent nicroparticles is given by Eq. 10 [42,43]

$$F_c = -C\pi\varepsilon_l f_{CM}^2 E^2 \tag{10}$$

where the coefficient C ranges from 3 to $>10^3$ depending on the distance between the yeast cells and the length of the microparticle chain [44]. E is the electric field strength. ε_l is the real part of the permittivity of the medium, and the effective microparticle polarizability is determined by the Clausius–Mossotti (CM) factor;

$$f_{CM}(\omega) = \frac{\left(\tilde{\varepsilon}_p - \tilde{\varepsilon}_l\right)}{\left(\tilde{\varepsilon}_p + 2\tilde{\varepsilon}_l\right)} \tag{11}$$

$$\tilde{\varepsilon}_{p,l} = \varepsilon_{p,l} - j\left(\frac{\sigma_{p,l}}{\omega}\right) \tag{12}$$

where the subscripts p and l correspond to the microparticle and medium, respectively. $\tilde{\varepsilon}_{p,l}$ is the complex permittivity of microparticle or medium, $\varepsilon_{p,l}$ and σ are the permittivity and electric conductivity of micoparticle or medium.

The F_a is zero in the PNs, while the F_c is the largest. Therefore, the F_a drives yeast cells to the PNs to form a line, and the F_c drives yeast cells to the lower electric field (pressure anti-nodes) to form a line along PN line [45] (e.g., the dots between lines in Fig. 8(c)). Under the interaction of the F_a and the F_c, yeast cells are forced to form array of lines and dots on the xy plane (Fig. 8(c)).

According to Eq. 10, the F_c is positively correlated with electric field strength E, so the

effect of chain force is more significant in 3D line arrays due to the higher power in 3D experiments. F_c is linearly proportional to the in-phase microparticle polarizability, which can be affected by the solution conductivity [42]. When the conductivity of the solution increases, the in-phase microparticle polarizability decreases, thus the F_c force between adjacent particles decreases. Inserting a metal layer between the substrate and chamber can shield the microparticles from the electric field, and decrease the F_c. Therefore, we can realize 3D line arrays of yeast cells more precisely by appropriately reducing the power, improving the conductivity of the solution or inserting a metal layer between substrate and chamber.

4. Conclusions

In summary, we have demonstrated in this paper that 3D patterning of lines of microparticles can be achieved in ZnO/Si SAW devices using SSAWs. We systematically investigated the effects of SSAW frequency, channel width and thickness on 3D line patterns. We have also achieved precise position control of the microparticles in the direction of SAW propagation by changing the phase angles of the SAW. We realized and observed the 3D patterning of lines of yeast cells. It is an important biomedicine-related application in microarrays, tissue engineering and regenerative medicine. Moreover, a numerical model has been developed to investigate the SAW acoustic field and the 3D motions of microparticles under the acoustic radiation forces within a microchamber.

Acknowledgement

The authors gratefully acknowledge the support of Research and Development Program of China [grant number 2016YFB0402705]; Shenzhen Science & Technology Project [grant numbers JCYJ20170817100658231, JCYJ20180507182439574, JCYJ20180305124317872]; Shenzhen Key Lab Fund [grant number ZDSYS20170228105421966]; UK Engineering and Physical Sciences Research Council (EPSRC) [grant number EP/P018998/1]; Newton Mobility [grant number IE161019] through Royal Society and the National Natural Science Foundation of China, Zhejiang Provincial Public Technology Research and Social Development Project [grant number LGF19F010007].

References

[1] T.D. Nguyen, V.T. Tran, Y.Q. Fu, H. Du, Patterning and manipulating microparticles into a three-dimensional matrix using standing surface acoustic waves, Appl. Phys. Lett. 112 (2018) 213507. doi:10.1063/1.5024888.

[2] X. Ding, P. Li, S.-C.S. Lin, Z.S. Stratton, N. Nama, F. Guo, D. Slotcavage, X. Mao, J. Shi, F. Costanzo, T.J. Huang, Surface acoustic wave microfluidics, Lab Chip. 13 (2013) 3626–3649. doi:10.1039/C3LC50361E.

[3] M.C. Jo, R. Guldiken, Particle manipulation by phase-shifting of surface acoustic waves, Sensors Actuators A Phys. 207 (2014) 39–42.

[4] W. Connacher, N. Zhang, A. Huang, J. Mei, S. Zhang, T. Gopesh, J. Friend, Micro/nano acoustofluidics: materials, phenomena, design, devices, and applications, Lab Chip. 18 (2018) 1952–1996. doi:10.1039/C8LC00112J.

[5] A. Ozcelik, J. Rufo, F. Guo, Y. Gu, P. Li, J. Lata, T.J. Huang, Acoustic tweezers for the life sciences, Nat. Methods. 15 (2018) 1021–1028. doi:10.1038/s41592-018-0222-9.

[6] Y. Liu, Y. Li, A.M. el-Hady, C. Zhao, J.F. Du, Y. Liu, Y.Q. Fu, Flexible and bendable acoustofluidics based on ZnO film coated aluminium foil, Sensors Actuators B Chem. 221 (2015) 230–235. doi:10.1016/J.SNB.2015.06.083.

[7] S.R. Heron, R. Wilson, S.A. Shaffer, D.R. Goodlett, J.M. Cooper, Surface Acoustic Wave Nebulization of Peptides As a Microfluidic Interface for Mass Spectrometry, Anal. Chem. 82 (2010) 3985–3989. doi:10.1021/ac100372c.

[8] X.Y. Du, Y.Q. Fu, S.C. Tan, J.K. Luo, A.J. Flewitt, W.I. Milne, D.S. Lee, N.M. Park, J. Park, Y.J. Choi, S.H. Kim, S. Maeng, ZnO film thickness effect on surface acoustic wave modes and acoustic streaming, Appl. Phys. Lett. 93 (2008) 94105. doi:10.1063/1.2970960.

[9] G. Destgeer, H.J. Sung, Recent advances in microfluidic actuation and micro-object manipulation via surface acoustic waves, Lab Chip. 15 (2015) 2722–2738. doi:10.1039/C5LC00265F.

[10] D.B. Go, M.Z. Atashbar, Z. Ramshani, H.-C. Chang, Surface acoustic wave devices for chemical sensing and microfluidics: a review and perspective, Anal. Methods. 9 (2017) 4112–4134. doi:10.1039/C7AY00690J.

[11] J. Shi, X. Mao, D. Ahmed, A. Colletti, T.J. Huang, Focusing microparticles in a microfluidic channel with standing surface acoustic waves (SSAW), Lab Chip. 8 (2008) 221–223. doi:10.1039/B716321E.

[12] A. Nilsson, F. Petersson, H. Jönsson, T. Laurell, Acoustic control of suspended particles in micro fluidic chips, Lab Chip. 4 (2004) 131–135. doi:10.1039/B313493H.

[13] J. Takagi, M. Yamada, M. Yasuda, M. Seki, Continuous particle separation in a microchannel having asymmetrically arranged multiple branches, Lab Chip. 5 (2005) 778–784. doi:10.1039/B501885D.

[14] D.H. Yoon, J.B. Ha, Y.K. Bahk, T. Arakawa, S. Shoji, J.S. Go, Size-selective separation of micro beads by utilizing secondary flow in a curved rectangular microchannel, Lab Chip. 9 (2009) 87–90. doi:10.1039/B809123D.

[15] J. Shi, H. Huang, Z. Stratton, Y. Huang, T.J. Huang, Continuous particle separation in a microfluidic channelvia standing surface acoustic waves (SSAW), Lab Chip. 9 (2009) 3354–3359. doi:10.1039/B915113C.

[16] X. Ding, S.-C.S. Lin, M.I. Lapsley, S. Li, X. Guo, C.Y. Chan, I.-K. Chiang, L. Wang, J.P. McCoy, T.J. Huang, Standing surface acoustic wave (SSAW) based multichannel cell sorting, Lab Chip. 12 (2012) 4228–4231. doi:10.1039/C2LC40751E.

[17] B.W. Drinkwater, Dynamic-field devices for the ultrasonic manipulation of microparticles, Lab Chip. 16 (2016) 2360–2375. doi:10.1039/C6LC00502K.

[18] D.J. Collins, C. Devendran, Z. Ma, J.W. Ng, A. Neild, Y. Ai, Acoustic tweezers via sub–time-of-flight regime surface acoustic waves, Sci. Adv. 2 (2016) e1600089. doi:10.1126/sciadv.1600089.

[19] V. Marx, Biophysics: using sound to move cells, Nat. Methods. 12 (2015) 41–44.

[20] J. Shi, S. Yazdi, S.-C. Steven Lin, X. Ding, I.-K. Chiang, K. Sharp, T.J. Huang, Three-dimensional continuous particle focusing in a microfluidic channelvia standing surface acoustic waves (SSAW), Lab Chip. 11 (2011) 2319–2324. doi:10.1039/C1LC20042A.

[21] J. Zhou, X. Tao, J. Luo, Y. Li, H. Jin, S. Dong, J. Luo, H. Duan, Y. Fu, Nebulization using ZnO/Si surface acoustic wave devices with focused interdigitated transducers, Surf. Coatings Technol. 367 (2019) 127–134. doi:https://doi.org/10.1016/j.surfcoat.2019.03.078.

[22] Y.Q. Fu, J.K. Luo, N.T. Nguyen, A.J. Walton, A.J. Flewitt, X.T. Zu, Y. Li, G. McHale, A. Matthews, E. Iborra, H. Du, W.I. Milne, Advances in piezoelectric thin films for acoustic biosensors, acoustofluidics and lab-on-chip applications, Prog. Mater. Sci. 89 (2017) 31–91. doi:https://doi.org/10.1016/j.pmatsci.2017.04.006.

[23] G. Wingqvist, AlN-based sputter-deposited shear mode thin film bulk acoustic resonator (FBAR) for biosensor applications — A review, Surf. Coatings Technol. 205 (2010) 1279–1286. doi:https://doi.org/10.1016/j.surfcoat.2010.08.109.

[24] Y.Q. Fu, J.K. Luo, X.Y. Du, A.J. Flewitt, Y. Li, G.H. Markx, A.J. Walton, W.I. Milne, Recent developments on ZnO films for acoustic wave based bio-sensing and microfluidic applications: a review, Sensors Actuators B Chem. 143 (2010) 606–619. doi:https://doi.org/10.1016/j.snb.2009.10.010.

[25] J. Hao, T. Xiang, S. Dong, Y. Qin, L. Yu, J. Luo, M.J. Deen, Flexible surface acoustic wave respiration sensor for monitoring obstructive sleep apnea syndrome, J. Micromechanics Microengineering. 27 (2017).

[26] C.D. Wood, S.D. Evans, J.E. Cunningham, R. O'Rorke, C. Wälti, A.G. Davies, Alignment of particles in microfluidic systems using standing surface acoustic waves, Appl. Phys. Lett. 92 (2008) 44104. doi:10.1063/1.2838748.

[27] L. Johansson, J. Enlund, S. Johansson, I. Katardjiev, V. Yantchev, Surface acoustic wave induced particle manipulation in a PDMS channel—principle concepts for continuous flow applications, Biomed. Microdevices. 14 (2012) 279–289. doi:10.1007/s10544-011-9606-7.

[28] K. Wang, W. Zhou, Z. Lin, F. Cai, F. Li, J. Wu, L. Meng, L. Niu, H. Zheng, Sorting of tumour cells in a microfluidic device by multi-stage surface acoustic waves, Sensors Actuators B Chem. 258 (2018) 1174–1183. doi:10.1016/J.SNB.2017.12.013.

[29] D. Hartono, Y. Liu, P.L. Tan, X.Y.S. Then, L.-Y.L. Yung, K.-M. Lim, On-chip measurements of cell compressibility via acoustic radiation, Lab Chip. 11 (2011) 4072–4080. doi:10.1039/C1LC20687G.

[30] C. Bouyer, P. Chen, S. Güven, T.T. Demirtaş, T.J.F. Nieland, F. Padilla, U. Demirci, A Bio-Acoustic Levitational (BAL) Assembly Method for Engineering of Multilayered, 3D Brain-Like Constructs, Using Human Embryonic Stem Cell Derived Neuro-Progenitors, Adv. Mater. 28

(2016) 161–167. doi:10.1002/adma.201503916.

[31] N.D. Orloff, J.R. Dennis, M. Cecchini, E. Schonbrun, E. Rocas, Y. Wang, D. Novotny, R.W. Simmonds, J. Moreland, I. Takeuchi, J.C. Booth, Manipulating particle trajectories with phase-control in surface acoustic wave microfluidics, Biomicrofluidics. 5 (2011) 44107. doi:10.1063/1.3661129.

[32] L. Meng, F. Cai, Z. Zhang, L. Niu, Q. Jin, F. Yan, J. Wu, Z. Wang, H. Zheng, Transportation of single cell and microbubbles by phase-shift introduced to standing leaky surface acoustic waves, Biomicrofluidics. 5 (2011) 44104. doi:10.1063/1.3652872.

[33] L. Meng, F. Cai, F. Li, W. Zhou, L. Niu, H. Zheng, Acoustic tweezers, J. Phys. D. Appl. Phys. 52 (2019) 273001. doi:10.1088/1361-6463/ab16b5.

[34] R. Kishor, Z. Ma, S. Sreejith, Y.P. Seah, H. Wang, Y. Ai, Z. Wang, T.-T. Lim, Y. Zheng, Real time size-dependent particle segregation and quantitative detection in a surface acoustic wave-photoacoustic integrated microfluidic system, Sensors Actuators B Chem. 252 (2017) 568–576. doi:10.1016/J.SNB.2017.06.006.

[35] J. Shi, D. Ahmed, X. Mao, S.-C.S. Lin, A. Lawit, T.J. Huang, Acoustic tweezers: patterning cells and microparticles using standing surface acoustic waves (SSAW), Lab Chip. 9 (2009) 2890–2895. doi:10.1039/B910595F.

[36] C.P. Kurtzman, J.W. Fell, Yeast Systematics and Phylogeny — Implications of Molecular Identification Methods for Studies in Ecology BT - Biodiversity and Ecophysiology of Yeasts, in: G. Péter, C. Rosa (Eds.), Springer Berlin Heidelberg, Berlin, Heidelberg, 2006: pp. 11–30. doi:10.1007/3-540-30985-3_2.

[37] C.S. Hoffman, V. Wood, P.A. Fantes, An Ancient Yeast for Young Geneticists: A Primer on the Schizosaccharomyces pombe Model System, Genetics. 201 (2015) 403–423. doi:10.1534/genetics.115.181503.

[38] X. Chen, Z.-H. Jiang, S. Chen, W. Qin, Microbial and bioconversion production of D-xylitol and its detection and application, Int. J. Biol. Sci. 6 (2010) 834–844. https://www.ncbi.nlm.nih.gov/pubmed/21179590.

[39] F. Thevenieau, J.M. Nicaud, C. Gaillardin, Yeast Biotechnology: Diversity and Applications, Yeast Biotechnol. Divers. Appl. (2009) 590–613.

[40] D. Botstein, G.R. Fink, Yeast: an experimental organism for 21st Century biology, Genetics. 189 (2011) 695–704. doi:10.1534/genetics.111.130765.

[41] G.G. Stewart, F.G. Priest, Handbook of Brewing, Second Edition, CRC Press, 2006. https://books.google.co.jp/books?id=TIYbNdrIsPEC.

[42] T. Zheng, C. Wang, C. Xu, Q. Hu, S. Wei, Patterning microparticles into a two-dimensional pattern using one column standing surface acoustic waves, Sensors Actuators A Phys. 284 (2018) 168–171. doi:https://doi.org/10.1016/j.sna.2018.10.001.

[43] O.D. Velev, K.H. Bhatt, On-chip micromanipulation and assembly of colloidal particles by electric fields, Soft Matter. 2 (2006) 738–750. doi:10.1039/B605052B.

[44] K. Kendall, Electromechanics of particles : T.B. Jones, published by Cambridge University Press, Cambridge, UK, 1995, 265 pp., £40.00 ($64.95), ISBN 0-521-43196-4, Powder Technol. 89 (1996) 177–178.

[45] N.G. Green, Dielectrophoresis and AC Electrokinetics BT - Electrokinetics and Electrohydrodynamics in Microsystems, in: A. Ramos (Ed.), Springer Vienna, Vienna, 2011: pp. 61–84. doi:10.1007/978-3-7091-0900-7_3.